Characterizing the Footprint of Eddy Covariance System and Large Aperture Scintillometer Measurements to Validate Satellite-Based Surface Fluxes

Jie Bai, Li Jia, Shaomin Liu, Ziwei Xu, Guangcheng Hu, Mingjia Zhu, and Lisheng Song

***Abstract*—To validate satellite-based surface fluxes by ground measurements properly, several numerical simulations were carried out at a homogeneous alpine meadow site and mixed cropland site, considering various atmospheric conditions and different land cover distribution types. By comparing various pixel selection methods, the results showed that footprint was significant in insuring a consistent spatial scale between ground measurements and satellite-based surface fluxes, particularly for heterogeneous surface and high-resolution remote sensing data. Because large aperture scintillometer measurements cover larger areas than eddy covariance (EC) system measurements, the spatial heterogeneity at a subpixel scale in complicated surface should be further considered in validating coarse satellite data. Thus, more accurate validation data and scaling methods must be developed, such as measuring surface fluxes at the satellite pixel scale by a flux measurement matrix or airborne EC measurements.**

***Index Terms*—Flux measurement, footprint, remote sensing, scale, validation.**

I. Introduction

UNDERSTANDING the temporal and spatial distributions of surface heat fluxes, including sensible heat flux and latent heat flux, is critical in irrigation management, crop yield forecasting, large-scale meteorological research, and climatology forecasting and application.

Many techniques based on ground-based measurements of surface fluxes have led to an improved understanding of soil–vegetation–atmosphere transfer processes. However, these ground measurement systems having limited instantaneous fields of view do not provide spatial variation of surface heat fluxes at a large scale compared with remote sensing estimations. Although remote sensing data provides space continuous surface flux estimation, a series of factors limited the accuracy of satellite-based surface fluxes [1]. Thus, a reasonable and reliable validation method based on ground-based measurement is critical.

Fixed point or patch measurements have numerous uncertainties in validating satellite-based surface flux estimation, including the measurement errors in point or patch scale and spatial scaled mismatch errors, whereas the latter one is the main difficulty in validation. The mismatch error in spatial scale is mainly caused by surface heterogeneity and nonlinear relationship between surface parameters and surface fluxes [2], [3]. As a result, a pixel selection method is significant in validation. Generally, the single pixel where the instrument is located, or several pixels surrounding the instrument location are defined as pixels to be validated, then the single pixel value or the average of multiple pixels are taken as satellite-based estimations to be compared with ground measurements. Comparing with the aforementioned two-pixel selection methods, the selection method based on the footprint of flux measurement solves the problem of scaled mismatch between ground measurements and satellite-based estimations to a certain extent [4], [5]. However, the complicated issues of this method is the shape, size, and orientation of footprint are variable, which are affected by the instrument heights of eddy covariance (EC) system/large aperture scintillometer (LAS) (and path length of LAS), wind speed/direction, atmospheric stability, and surface conditions. So far, the effects of the aforementioned factors on matching satellite-based surface flux estimation with ground-based measurements have not been evaluated yet.

Using the homogeneous A'Rou (AR) site and mixed crop land of the Guantao (GT) site as examples, EC/LAS measurements and their corresponding footprints were used to validate the estimated surface fluxes from Landsat Thematic Mapper (TM) and Advanced Along Track Scanning Radiometer (AATSR) data. Several pixel selection methods were compared over different land cover distribution types, in hopes of finding the best method for validating satellite-based surface fluxes over heterogeneous surface.

Manuscript received January 28, 2014; revised June 9, 2014 and September 28, 2014; accepted October 30, 2014. This work was supported by the National Natural Science Foundation of China under Grant 91125002 and by the European Commission (Call FP7-ENV-2007-1) under Grant 212921. *(Corresponding author: Shaomin Liu.)*

J. Bai is with the State Key Laboratory of Remote Sensing Science, Beijing Normal University, Beijing 100875, China, and also with China TopRS Technology Co. Ltd., Beijing 100039, China (e-mail: baijie126126@126.com).

L. Jia and G. Hu are with the State Key Laboratory of Remote Sensing Science, Institute of Remote Sensing and Digital Earth, Chinese Academy of Sciences, Beijing 100101, China (e-mail: jiali@radi.ac.cn; hugc@radi.ac.cn).

S. Liu, Z. Xu, M. Zhu, and L. Song are with the State Key Laboratory of Remote Sensing Science, Beijing Normal University, Beijing 100875, China (e-mail: smliu@bnu.edu.cn; xuzw@bnu.edu.cn; hainingkim@163.com; scausls@163.com).

Color versions of one or more of the figures in this paper are available online at http://ieeexplore.ieee.org.

Digital Object Identifier 10.1109/LGRS.2014.2368580

II. Study Area and Data Acquisition

A. Study Area

The study areas cover two different land types in China. The AR site is located in the upper reaches of the Heihe River Basin in northwest China. Ground measurements performed at site AR since March 2008 are parts of the Watershed Allied Telemetry Experimental Research (WATER) [6]. The land surface is covered by alpine meadow, which turns to green in May and withers until September. The other site used in this letter is GT, located in the northern part of Hai River Basin in China. Field measurements have been performed there since August 2007 over mixed crop land and residential areas. The experiment taken at site GT is part of the multiscale surface flux and meteorological elements measurement experiment in the Hai River Basin [7]. Winter wheat, maize, and cotton are the main crop types; the maize begins to grow after the winter wheat harvest in mid-June. The growing period for cotton is from May to September.

B. Data Acquisition

A complete set of ground measurements was performed at both sites simultaneously using an Automatic Weather System (AWS), EC, and LAS. The installation height of EC was 3.15 and 15.6 m at sites AR and GT, respectively. Raw EC data were stored at a sampling frequency of 10 Hz and processed using the postprocessing software Edire (http://www.geos.ed.ac.uk/abs/research/micromet/EdiRe), including spike removal, lag correction of H_2O/CO_2 relative to the vertical wind component, sonic virtual temperature correction, the performance of the planar fit coordinate rotation, corrections for density fluctuation (Webb-Pearman-Leuning (WPL) correction), frequency response correction, etc. Then, energy balance closure correction was done before EC data used for validation. LAS data were recorded every 1 min at site AR using a Scintec BLS450 LAS and every 10 min at site GT using a Kipp & Zonen LAS. The effective height and path length were 9.5 and 2390 m at site AR, 15.6 and 2760 m at site GT, respectively. Recorded LAS data were carefully screened and processed to ensure the data quality, including data screening, and humidity correction with Bowen Ratio. Meanwhile, the stability function f_T was defined according to Andreas (1988) [7]. The EC and LAS data were processed with an averaging time of 30 min, their calculation details are provided in [8] and [9]. The AWS at each site included data of precipitation, wind speed/direction, air temperature/humidity, air pressure, radiation, soil heat flux, etc. All of the AWS data were collected for each 10 s and stored at 10-min intervals.

Both Landsat TM data (30-m resolution) and AATSR data (approximately 1080-m resolution) were collected on two different days at both sites. At site AR, the data were acquired at approximately 12:00 BST (Beijing Standard Time) for TM data and approximately 11:30 BST for AATSR data on July 7 and July 23, 2008, which were in the grass growing season. At site GT, TM data at approximately 11:00 BST and AATSR at approximately 10:00 BST were acquired for different land cover distribution types. The first image depicted winter wheat and cotton at the emergence stage on May 17, 2009. The second image depicted harvest-stage winter wheat and growing cotton on June 2, 2009. In our study, the Landsat TM data on July 7, 2008 at site AR and June 2, 2009 at site GT were selected to represent the fixed background land cover in following numerical simulation, both of the Landsat TM and AATSR data at both sites were used in validation by ground-based measurements.

III. Methods

A. Footprint Model

Flux footprint can be used to describe the function between the spatial distributions of source/sink of fluxes and measurements within the surface layer. By determining the footprint, the source area that mainly contributes to the ground flux measurements is defined, and the relative contribution within it can also be acquired. In our study, the Eulerian analytical expression [10] was used to obtain EC flux footprint. The flux footprint model for LAS was constructed based on the 2-D point-flux footprint function of EC and the path-weighting function of LAS [11], [12]. We chose a 6 km $\times$ 6 km area to approximate the total source area around the measurement point for EC and the central part of the LAS optical path, respectively. The spatial resolutions of EC and LAS footprint were roughly equal to their measurement height, respectively [13], which are 3 m for EC footprint and 10 m for LAS footprint at site AR, 15 m for EC and LAS footprint at site GT. The footprint-integrated fluxes were averaged over the area that lies within the contour that encompasses the 95% contribution.

B. Satellite-Based Surface Flux Estimation Model

The Surface Energy Balance System (SEBS) model uses remote sensing data and meteorological information to estimate surface sensible and latent heat fluxes based on the surface energy balance equation [14]. Using the SEBS model, the sensible heat flux can be obtained through the iteration of a series of nonlinear equations by constraining values for the wet and dry limit cases.

C. Pixel Selection Method

For remote sensing data of Landsat TM and AATSR, one to several pixels are covered by EC or LAS source area, which are defined as pixels to be validated. Meanwhile, more than one footprint grid is included in each TM or AATSR pixel, thus all the relative weight of footprint grid within each satellite pixel should be accumulated first. The footprint-integrated sensible heat flux for EC or LAS source area (H_{FP}) can be calculated as

$$H_{\mathrm{FP}} = \sum_{i=1}^{n} H_i \times f_{\mathrm{RW\_}i} \tag{1}$$

where n is the number of remote sensing pixel covered by EC or LAS source area, H_i is the ith pixel value, and $f_{\mathrm{RW\_}i}$ is the relative weight corresponding to ith pixel.

TABLE I
PARAMETERS OF DIFFERENT ATMOSPHERE CONDITIONS AT SITES AR AND GT

Site	Footprint	Wind Direction (°)	Wind Speed (m/s)	Obukhov Length (m)	The upwind distance (m)
AR	EC/LAS_1	74.3/104.8	2.9/3.7	-14.0	323/1149
	EC/LAS_2	114.8/130.5	3.0/2.5	-40.0	469/725
	EC/LAS_3	138.4/181.0	0.8/1.2	-2.4	169/391
	EC/LAS_4	281.2/278.7	4.5/2.9	-109.2	436/1471
	EC/LAS_5	291.6/307.7	4.3/5.6	-31.6	465/1556
	EC/LAS_6	330.3/355.1	1.0/1.6	-0.9	134/499
GT	EC/LAS_1	9.7	7.0	-115.2	1484/725
	EC/LAS_2	84.8	2.2	-4.4	429/545
	EC/LAS_3	138.7	4.4	-112.2	1724/1630
	EC/LAS_4	170.1	2.5	-20.4	713/513
	EC/LAS_5	187.7	2.6	-53.1	867/510
	EC/LAS_6	200.9	3.1	-118.0	1092/722

*Different wind speeds / directions at EC and LAS measurement height were applied for the EC and LAS footprints at site AR, respectively. EC/LAS_1 through EC/LAS_6 stands for the six different EC and LAS footprints for sites AR and GT. The upwind distance indicates the distance between EC tower or the middle point of LAS path and the far end of the contour encompassing 95% footprint contribution along wind direction for EC or LAS footprint, respectively.

IV. RESULT AND ANALYSIS

The variation of flux source area is related to the instrument height (and path length for LAS), atmospheric condition, and surface conditions. The instrument height and LAS path length were fixed prior to taking the measurements. Therefore, this letter focuses on the impact of other factors on the footprint-integrated flux by numerical simulation, including the different atmospheric conditions (e.g., atmosphere stability, wind speed, and direction) and land cover distribution types.

A. Atmospheric Conditions

Due to the limitation of satellite data and atmospheric condition (e.g., cloudy, rainy), a relatively small number of satellite data can be obtained during our experiments, particularly for Landsat TM data. In order to sufficiently explore the relationship between variable atmospheric conditions and the shape, size, and orientation of the footprint, six atmospheric conditions are selected based on ground measurements at satellite passing time on July 2008 for site AR and June 2009 for site GT, by assuming the actual sensible heat fluxes are uninfluenced by atmospheric turbulence and footprints.

The selection of atmospheric conditions for both sites is done according to: 1) covering the variation range of wind speeds and wind directions over different land cover distributions; and 2) covering the variation range of atmospheric stability for similar wind direction. Detailed parameters of atmospheric conditions and the upwind distance between the EC tower or the middle point of LAS path and the far end of the contour encompassing 95% footprint contribution along wind direction are listed in Table I.

Due to different atmospheric conditions, the flux source area varies (see Fig. 1). Taking LAS footprint at site AR as an example [see Fig. 1(b)], both the wind speed and the absolute value of the Obukhov length for LAS_3 are less than LAS_4; thus, the source area for LAS_3 is much smaller and narrower

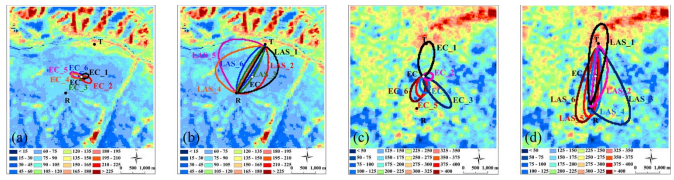

Fig. 1. Variation of multitime EC and LAS footprints over TM-estimated sensible heat flux ($W \cdot m^{-2}$) by (a) and (b) SEBS on July 7, 2008 at site AR and (c) and (d) on June 2, 2009 at site GT; EC/LAS_1 through EC/LAS_6 stand for the six different EC and LAS footprints for sites AR and GT.

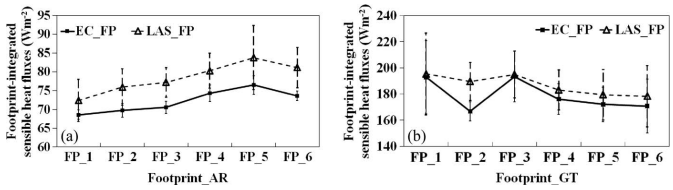

Fig. 2. Variation of footprint-integrated sensible heat fluxes for multitime EC and LAS footprints over TM-estimated sensible heat flux ($W \cdot m^{-2}$) by (a) SEBS on July 7, 2008 at site AR and (b) on June 2, 2009 at site GT ; FP_1 through FP_6 stand for the six different EC and LAS footprints for sites AR and GT. Error bar stands for the standard error of the estimated sensible heat flux among the pixels within EC or LAS footprint.

accordingly. Meanwhile, the wind direction for LAS_3 differs from that of LAS_4, the surface heat conditions are obviously different. Most pixel values within LAS_3 are in the ranges of 60–75 $W \cdot m^{-2}$, while the pixels included in LAS_4 are mainly between 75 and 90 $W \cdot m^{-2}$, some pixels with higher sensible heat flux in the northern mountain area are also included in LAS_4. As a result, according to the variation of atmospheric conditions, the orientation, shape, and size of source area are varied, which lead to the changing in the fluxes as seen by the sensor accordingly.

Furthermore, with a fixed flux map of sites AR and GT, the footprint-integrated sensible heat fluxes for different EC and LAS footprints are calculated for more specific comparison (see Fig. 2). Thus, any difference between the six cases is solely due to variations in the footprint at both sites AR and GT. Generally, compared with EC footprint, the source area of LAS footprint includes more bare soil, road and mountains at site AR, and more roads and villages at site GT. Thus, the LAS-derived sensible heat fluxes are larger than that of the EC derived for all conditions. Meanwhile, integrated with the distribution of surface condition and footprint, the footprint-integrated sensible heat flux of LAS_4 is obviously larger than LAS_3. The similar performances between varied atmospheric conditions and the variation of footprints, as well as footprint-integrated sensible heat fluxes also can be found for EC and LAS footprint at site GT. What is more, with the increasing complexity at site GT, the heterogeneity among different source areas becomes more significant.

B. Land Cover Distribution Types

For a better understanding the effects of various land distribution types on validating satellite-based surface fluxes by ground measurements, three different land cover distribution types (Types *A*, *B*, and *C*) based on Landsat TM data on

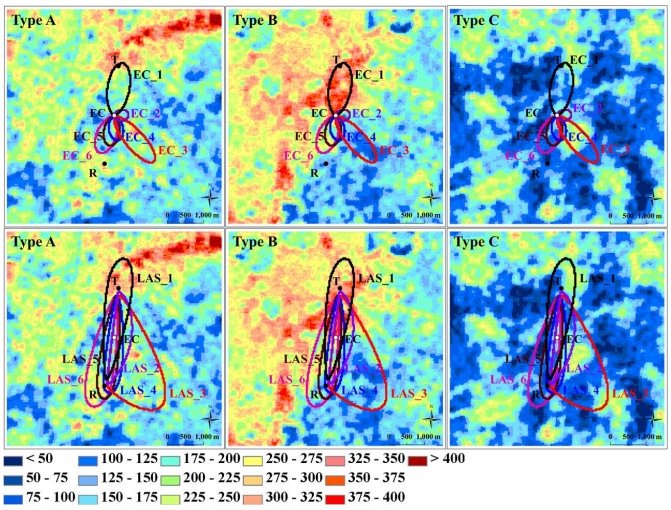

Fig. 3. Spatial sampling obtained at Types *A* (left), *B* (middle), and *C* (right) for site GT with the EC (top) and LAS (bottom) systems; image of the sensible heat flux ($\mathrm{W \cdot m^{-2}}$) estimated with TM by SEBS on June 2, 2009 at site GT as reference (6 km × 6 km); EC/LAS_1 through EC/LAS_6 are the same to Fig. 1.

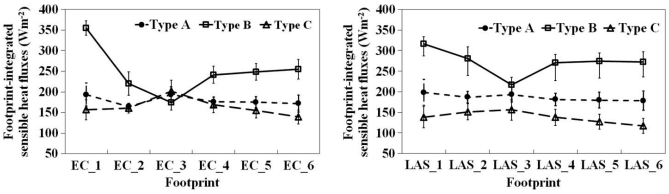

Fig. 4. Variation of footprint-integrated sensible heat fluxes for multitime EC (a) and LAS (b) footprints over TM-estimated sensible heat flux ($\mathrm{W \cdot m^{-2}}$) by SEBS on June 2, 2009 at Types A, B, and C of site GT; EC/LAS_1 through EC/LAS_6 stand for the six different EC and LAS footprints for site GT. Error bar stands for the standard error of the estimated sensible heat flux among the pixels within EC or LAS footprint.

June 2, 2009 at site GT are settled (see Fig. 3). While Type A is the real situation of Landsat TM data, Types B and C are simulated by moving the EC/LAS towers and their associated footprints northward and southward by 6 km, respectively. The area in Type *B* is much drier in the north of the EC and LAS towers. For Type *C*, patches of different land covers are cross distributed around the EC and LAS system.

Combined with the aforementioned six different atmospheric conditions, the effect of surface heterogeneity on the footprint-integrated surface fluxes are simulated and discussed. As the change of land cover distribution types, the surface heat conditions covered by each source area are obviously different (see Fig. 3). Thus, common validation ways of the single pixel value or the average of several fixed pixels are no longer applicable.

Further analysis is based on quantitative comparison of footprint-integrated sensible heat flux to deeply study the effects of land cover distribution on EC and LAS measurements. Fig. 4 gives the variation of six EC and LAS footprint-integrated sensible heat fluxes over three land cover distribution types.

By changing the footprint over each land cover distribution type, the difference between the maximum and minimum footprint-integrated sensible heat flux among six footprint cases, defined as variation range, is used to evaluate the effects of footprint on integrated sensible heat fluxes. The variation range of EC footprint-integrated sensible heat fluxes for the six atmospheric conditions were 28.8, 180.7, and 62.3 $\mathrm{W \cdot m^{-2}}$ for Types *A*, *B*, and *C*, respectively. Because the LAS footprints covered much larger area, the integrated sensible heat fluxes were less affected by variable land cover distribution types. In our simulation, the variation ranges of LAS footprint-integrated sensible heat fluxes across the six atmospheric conditions were 20.0, 99.2, and 39.2 $\mathrm{W \cdot m^{-2}}$ for Types *A*, *B*, and *C*, respectively. Thus, Type *B* has the largest variability of footprint-integrated sensible heat flux, which is contradictory to the visual judgment that the heterogeneity of Type *C* seems to be larger than Types *A* and *B*.

Taking LAS footprint-integrated sensible heat fluxes as an example, the heterogeneity of various land cover distribution types would be further analyzed by footprint upwind distance. With the same measurement height, the LAS footprint upwind distance for each wind direction is the composite performance of varied atmospheric condition and surface roughness. Although the upwind distance of LAS footprint changes from 510 m to more than 1630 m (see Table I), the footprint-integrated sensible heat fluxes among six LAS footprints are relatively similar to each other for Types *A* and *C*, whereas they were obviously affected by the land cover of Type *B*, indicating a larger heterogeneity for this kind of land cover distribution.

Therefore, the determination of footprint is critical in considering the surface heterogeneity for the comparison of the satellite-based surface fluxes with EC or LAS measurements, particularly for complicated land cover distribution types. The analysis of land cover distribution effect would also be helpful in pixel selection.

C. Validation of Satellite-Based Surface Fluxes

Excepting for the shortcomings in the SEBS method, consistent spatial scale is significant in validation by matching ground measurements with remote sensing estimation. Several pixel selection methods were chosen for validating both TM and AATSR image data by comparing with EC and LAS measurements. The point method $(H_{\mathrm{EC\_Point}})$ and footprint-integrated method $(H_{\mathrm{EC\_FP}})$ were used for validation with EC measurements: 1) $H_{\mathrm{EC\_Point}}$, the pixel value of EC tower location; and 2) $H_{\mathrm{EC\_FP}}$, the footprint-integrated values from EC footprint by (1). Two different methods were used for validation with LAS measurements: 1) $H_{\mathrm{LAS\_mid\ point}}$, the pixel value of the middle point for the LAS path, the middle point is supposed to have the largest contribution to LAS measurement; and 2) $H_{\mathrm{LAS\_FP}}$, the footprint-integrated value from the LAS footprint by (1).

For the TM data validation illustrated in Fig. 5, the value of point method and footprint-integrated method are relatively consistent for the relative homogeneous surface at site AR. While for relatively heterogeneous surface of site GT, the greatest difference between $H_{\mathrm{EC\_Point}}$ and $H_{\mathrm{EC\_FP}}$ appears on GT_0602, $H_{\mathrm{EC\_FP}}$ is much closer to ground measurement. Statistically, the root-mean-square deviation (RMSD) values for $H_{\mathrm{EC\_Point}}$ and $H_{\mathrm{EC\_FP}}$ are 46.5 and 29.4 $\mathrm{W \cdot m^{-2}}$, respectively. The results demonstrate considering the source area

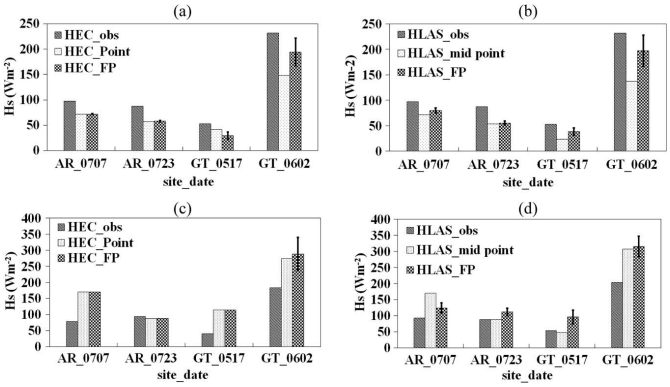

Fig. 5. Comparison of EC/LAS measurements and satellite-based sensible heat fluxes by SEBS at TM and AATSR passing time (site AR: July 7 and July 23, 2008; site GT: May 17 and June 2, 2009. Error bar stands for the standard error of the estimated sensible heat flux among the pixels within EC or LAS footprint).

of flux measurement and relative contribution of each pixel is particularly important for heterogeneous surface.

With regard to the validation of coarse spatial resolution AATSR data, both EC and LAS measurements are used to compare with the middle point method and the footprint-integrated method, respectively. Compared with the value of point method $(H_{\mathrm{LAS\_Point}})$, the value of footprint-integrated method is much closer to LAS measurements. Statistically, the RMSD values for $H_{\mathrm{LAS\_FP}}$ and $H_{\mathrm{LAS\_Point}}$ are 26.2 and 54.1 $\mathrm{W \cdot m^{-2}}$, respectively.

Moreover, the overall RMSD values for the validation of AATSR data with EC and LAS ground measurements are 79.6 and 61.9 $\mathrm{W \cdot m^{-2}}$, respectively for all four cases (AR_0707, AR_0723, GT_0517, GT_0602). Thus, taking the advantage of the regional measurement of the LAS system, the validation results for AATSR data should be more reliable than validation with EC measurements. However, the footprint is not well resolved at coarse resolution. The AATSR pixel cannot be fully covered by EC or LAS footprint, the pixel-mean flux is contaminated by the parts beyond EC or LAS source area. Therefore, to avoid large difference with ground measurements, the spatial heterogeneity at a subpixel scale should not be neglected at coarse resolution.

In addition to inconsistencies in spatial scale between ground measurement and satellite-based surface flux estimation, gaps in the temporal scale may also lead to differences in validation. The sensible heat fluxes measured by EC and LAS are averaged in 30 min, whereas the estimates from TM and AATSR data are instantaneous values. Therefore, the temporal mismatch between ground measurements and satellite-estimated fluxes should be also considered in validation.

V. Conclusion

This letter used numerical simulation to analyze the effect of footprint characteristics on matching ground measurements with satellite-based surface fluxes, by considering the influences of atmospheric condition and land cover distribution types. Results suggest the footprint is crucial in defining consistent spatial scale between ground measurements and satellite-based surface flux estimates in validation, particularly for heterogeneous surfaces and high-resolution remote sensing data. Since the coarse satellite pixel cannot be fully covered by EC or LAS flux footprint, further appropriate validation data with more consistent spatial representative is required in validating coarse satellite-based surface fluxes over complicated surface. The spatial heterogeneity at a subpixel scale over heterogeneous surface should be further considered. Consequently, measuring surface fluxes at the satellite pixel scale is urgent to be developed, by means of a flux measurement matrix or airborne eddy covariance measurements, etc.

References

[1] Z. Jia, S. Liu, Z. Xu, Y. Chen, and M. Zhu, "Validation of remotely sensed evapotranspiration over the Hai River Basin, China," *J. Geophys. Res.*, vol. 117, no. D13113, Jul. 2012.

[2] M. Choi, W. P. Kustas, and M. C. Anderson, "An intercomparison of three remote sensing-based surface energy balance algorithms over a corn and soybean production region (Iowa, US) during SMACEX," *Agric. Forest Meteorol.*, vol. 149, no. 12, pp. 2082–2097, Dec. 2009.

[3] N. A. Brunsell, J. M. Ham, and C. E. Owensby, "Assessing the multi-resolution information content of remotely sensed variables and elevation for evapotranspiration in a tall-grass prairie environment," *Remote Sens. Environ.*, vol. 112, no. 6, pp. 2977–2987, Jun. 2008.

[4] N. A. Brunsell, J. M. Ham, and K. A. Arnold, "Validating remotely sensed land surface fluxes in heterogeneous terrain with large aperture scintillometry," *Int. J. Remote Sens.*, vol. 32, no. 21, pp. 6295–6314, Jul. 2011.

[5] B. Z. Chen *et al.*, "Characterizing spatial representativeness of flux tower eddy-covariance measurements across the Canadian Carbon Program Network using remote sensing and footprint analysis," *Remote Sens. Environ.*, vol. 124, pp. 742–755, Sep. 2012.

[6] X. Li *et al.*, "Watershed allied telemetry experimental research," *J. Geophys. Res.*, vol. 114, no. D22103, Nov. 2009.

[7] E. L. Andreas, "Estimating Cn^2 over snow and sea ice from meteorological data," *J. Opt. Soc. Amer.*, vol. 5, no. 4, pp. 481–495, Apr. 1988.

[8] S. M. Liu, Z. W. Xu, Z. L. Zhu, Z. Z. Jia, and M. J. Zhu, "Measurements of evapotranspiration from eddy-covariance systems and large aperture scintillometers in the Hai River Basin, China," *J. Hydrol.*, vol. 487, pp. 24–38, Apr. 2013.

[9] S. M. Liu *et al.*, "A comparison of eddy-covariance and large aperture scintillometer measurements with respect to the energy balance closure problem," *Hydrol. Earth Syst. Sci.*, vol. 15, no. 4, pp. 1291–1306, Apr. 2011.

[10] R. Kormann and F. X. Meixner, "An analytical footprint model for non-neutral stratification," *Boundary Layer Meteorol.*, vol. 99, no. 2, pp. 207–224, May 2001.

[11] W. Meijninger *et al.*, "Determination of area-averaged sensible heat fluxes with a large aperture scintillometer over a heterogeneous surface-flevoland field experiment," *Boundary Layer Meteorol.*, vol. 105, no. 1, pp. 37–62, Oct. 2002.

[12] G. L. Peng, X. H. Cai, and S. M. Liu, "A flux footprint model for large aperture scintillometer" *[in Chinese with English abstract], Acta Sci. Nat. Univ. Pekinensis*, vol. 43, no. 6, pp. 822–827, Nov. 2007.

[13] A. Van de Boer, A. F. Moene, D. Schuttemeyer, and A. Graf, "Sensitivity and uncertainty of analytical footprint models according to a combined natural tracer and ensemble approach," *Agric. Forest Meteorol.*, vol. 169, pp. 1–11, Feb. 2013.

[14] Z. Su, "The Surface Energy Balance System (SEBS) for estimation of turbulent heat fluxes," *Hydrol. Earth Syst. Sci.*, vol. 6, pp. 85–100, 2002.